EASR

Engineering and Applied Science Research

https://www.tci-thaijo.org/index.php/easr/index

Published by the Faculty of Engineering, Khon Kaen University, Thailand

Properties of fly ash and rice husk ash blended geopolymer with sodium aluminate as activator solution

N. Shyamananda Singh[1)], Suresh Thokchom*[2)] and Rama Debbarma[1)]

[1)]Department of Civil Engineering, National Institute of Technology Agartala, Tripura 799046, India
[2)]Department of Civil Engineering, Manipur Institute of Technology, Manipur University, Imphal 795001, India

Received 3 April 2020
Revised 3 June 2020
Accepted 23 June 2020

Abstract

The study investigates properties of blended geopolymer based on fly ash (FA) and rice husk ash (RHA) activated with sodium aluminate as aluminum additive. Five series of geopolymer paste were studied with ratios of FA: RHA as 100:0, 75:25, 50:50, 25:75 and 0:100. Phase identification and quantification were performed by X-ray Diffraction (XRD). Fourier Transform Infrared Spectroscopy (FTIR), field emission scanning electron microscope (FESEM) were used to characterize the microstructure of the specimen. Quantification of the elements present were performed by Energy dispersion X-Ray Analysis (EDX). Compressive strength along with physical parameters such as bulk density, water absorption, sorptivity, apparent porosity was determined. Results shows that 25% replacement by RHA is the optimal percentage on physical-mechanical properties of the blended geopolymer. The finer particles of RHA filled the voids present in the geopolymer matrix through filling effect and enriched the gel which densify the specimen. SEM micrographs also validates the denser matrix of the specimen at the optimal replacement percentage. However, it was seen that blending of RHA with FA beyond the optimal 25% has a negative effect on the properties studied. The observation may be attributed due to the presence of zeolite X as confirmed by Quantitative XRD. Increase in the amount of zeolite X and its crystalline size has a negative impact on the compressive strength of the blended geopolymer. The present study is expected to provide a practical solution of utilizing FA and RHA solid waste in construction activities.

Keywords: Geopolymer, Fly ash, Rice husk ash, Quantitative XRD, FESEM, FTIR

1. Introduction

The issue of CO_2 emission with cement production led to the development of geopolymer, an alternate binder being first introduced by Davidovits [1]. Geopolymer are amorphous to semi crystalline three-dimensional aluminosilicate formed from raw materials rich in silica and aluminum [2]. Geopolymer precursors includes fly ash [3-5], metakaolin [6-8], silica [9, 10], rice husk ash [11], ground granulated blast furnace slag (GGBS) [12-14], calcined water treatment sludge [15]. These precursors were usually activated by hydroxides and silicates of sodium [16] and potassium [17].

Fly ash is one of the most widely used geopolymer precursor for its amorphous silica content. Around 800 million ton per annum of fly ash (FA) is produced word wide and India stand third after China and USA [18]. India generates about 196.44 million-ton fly ash from its thermal power plants with percentage utilization of 67.13% for the year 2017-2018 [19]. Based on these figures, there is around 64.57 million ton of fly ash which can be used as potential precursor for geopolymer production. Another silica rich source which has not been extensively explored for geopolymer applications is rice husk ash (RHA). Global production of rice is estimated to be about 782 million ton. India with 172.58 million ton is second in production for the year 2018 [20]. This generates around 34.58 million ton (about 20% of the production) of rice husk after milling. A small percentage of these are used in cement, refractory brick and as cattle feeds. The current disposal method is burning and dumping leading to the decomposition and other environmental issues. Utilization of RHA as rich source of silica can be considered in synthesis of geopolymer.

The properties of geopolymer depends on many factors particularly the relative ratio of silicon (Si) and aluminum (Al) [21, 22]. The prospect of blending FA and RHA geopolymer has been studied and reported to be have superior mechanical properties depending on fineness and blending percentage [23-25]. However, as the amount of partial replacement of FA by RHA is increased, the amount of silica in the geopolymer matrix is expected to increase. This will in turn tend to increase the Si/Al ratio. Sodium aluminate as aluminum additives can be provided to maintain the ratio of Si/Al. Previous researchers had reported that the addition of aluminate accelerate the process of geopolymer reaction leading to enhanced properties [26]. Sodium aluminate as activator has also been reported for fly ash based [27] and rice husk based geopolymers [22, 28, 29]. However, blended geopolymer based on FA and RHA activated by sodium aluminate is yet to be studied.

From the available literature, it is clear that FA and RHA are available in abundant quantities and can be utilized to produce blended geopolymer. Furthermore, limited studies have been reported on the properties of geopolymer with Al additives such as sodium aluminate. Therefore, the objective of the present work

*Corresponding author. Tel.: +9189 7402 7490
Email address: suresh@mitimphal.in; thoks1966@gmail.com
doi: 10.14456/easr.2021.11

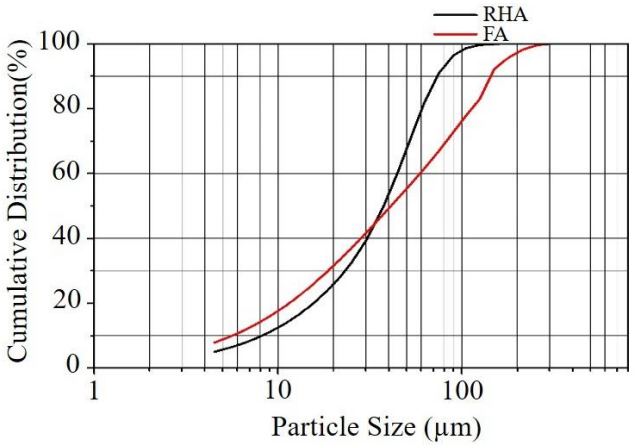

Figure 1 Particle Size Distribution of RHA and FA

Table 1 Chemical Composition of RHA and FA wt. %

Chemical Composition	RHA	FA
SiO_2	92.19	56.01
Al_2O_3	0.09	29.80
Fe_2O_3	0.10	3.58
TiO_2	0.71	1.75
MgO	0.41	0.30
K_2O	0.05	0.73
Na_2O	1.64	0.61
SO_3	0.41	-
CaO	0.09	2.36
P_2O_5	0.01	0.44
LOI	4.14	0.40

is to study the effect of blending percentage of FA and RHA on synthesis and engineering properties of geopolymer specimens. Feasibility of sodium aluminate as source of aluminum for FA and RHA blended geopolymer have also been investigated. The microstructure and chemical composition of the resulting geopolymers has been further characterized by FESEM/EDX, XRD and FTIR. The present research aims to add valuable contribution in the study of FA and RHA blended geopolymer for applications in infrastructure construction.

2. Experimental

2.1 Materials

Rice Husk ash (RHA), sourced from West Bengal, India were used for the study. Raw RHA were obtained after incinerating at 650-700°C for 1 hour and stored in air tight chamber [22, 24]. A 150 µm sieve was used to remove excessively large particles in RHA.

The sample are visually greyish white in colour. Particle size distribution of RHA are d_{10} =8.21µm, d_{50}=37.58µm and d_{90} =73.64µm as shown in Figure 1. Class F fly ash (FA) was procured from Kolaghat Thermal Power Plant, India. Particle size distribution of FA are d_{10} =5.66µm, d_{50}=41.30µm and d_{90} =164.71 µm as shown in Figure 1. The constituents of as received FA and RHA were determined by X-ray fluorescence (XRF) and tabulated in Table 1.

Scanning Electron Microscopy (SEM) shows the raw RHA with irregular, elongated nature of the microstructure in Figure 2(a). The SEM image of the as received FA is shown Figure 2 (b) where the particles are generally seen as spherical in shape.

For RHA based geopolymer, sodium aluminate supplied by Sigma–Aldrich was used as aluminum additive. The main constituents are Al (as Al_2O_3) (50-56%) and Na (as Na_2O) (40-45%). RHA and Sodium Aluminate were dry mixed and distilled water is added to the mixture. Raw RHA and FA are activated with a mixture of sodium hydroxide solutions and sodium aluminate. Merck India Private Ltd, India provided the sodium hydroxide in pellet form with 97% purity and specific gravity of 2.15. Sodium silicate solution was obtained from Loba Chemicals Ltd., India with Na_2O=14.7%, SiO_2=29.4%, and water 55.9% by mass.

2.2 Specimen preparation

Required quantities of FA and RHA was taken according to the proportion as given in Table 2. For unblended FA geopolymer, sodium hydroxide and sodium silicate solution were used as activator. A combination of sodium hydroxide and sodium aluminate as activator were specifically used for blended geopolymer. Sodium aluminate solution alone was used to activate unblended RHA geopolymer. The activator solution was prepared at least one day prior to its use. In a Hobart mixer, the activator was added to FA/RHA and allowed to mixed for 5 minutes to obtain a homogenous viscous paste. However, for blended geopolymer, FA and RHA were dry mixed together for 5 minutes prior to addition of activator [23]. Atomic ratios of Si/Al and Na/Al were kept constant at 2 and 1 respectively for all geopolymer paste specimens [22]. The oxide ratios (SiO_2/Al_2O_3) and (Na_2O/Al_2O_3) for the mixes works out to be constant at 2.3 and 0.7 respectively. The quantity of extra water added to each mix was based on obtaining geopolymer paste of comparable workability [24]. The fresh paste specimens were cast in 50 mm cube as per ASTM C-109-20a [30]. The specimens were precured for 1 hour at room temperature. Afterwards, the specimen were put in an oven at 80°C for 24 hours duration [29, 31]. The specimens were than demolded after cooling and then stored at room temperature till the day of testing. For all the parameters studied, the average of three samples were reported.

Mix proportions of the blended geopolymers specimens are presented in Table 2.

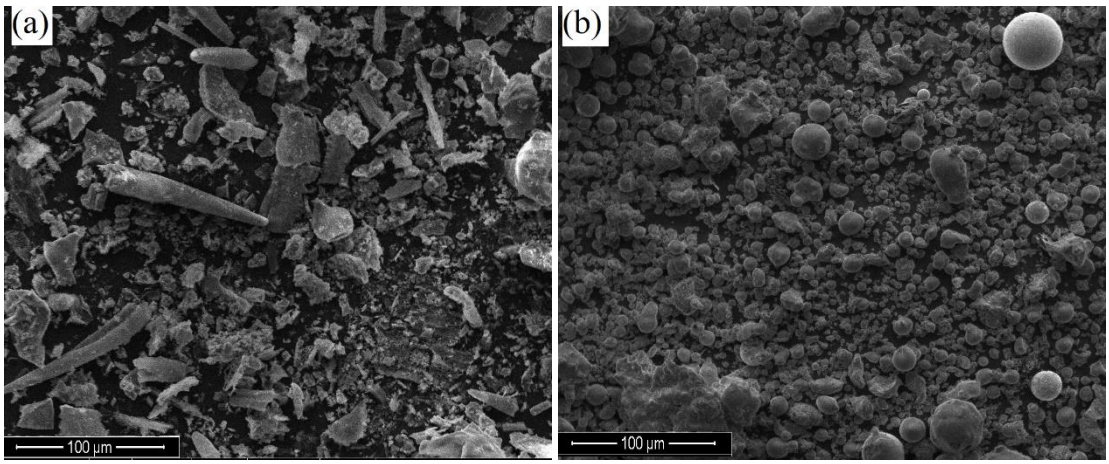

Figure 2 SEM micrograph of raw materials

Table 2 Batch composition of geopolymer (per 100 g of solid precursors)

Specimen ID	Atomic Ratios		Solid Precursors (g)		Activators (g)			Oxide Ratios		Extra water Added (g)
	Si/Al	Na/Al	FA	RHA	NaOH	Na_2SiO_3	Na_2AlO	SiO_2/Al_2O_3	Na_2O/Al_2O_3	
100FA	2	1	100	0	22.13	43.79	0.00	2.3	0.7	31.34
75FA	2	1	75	25	20.37	0.00	11.53	2.3	0.7	60.42
50FA	2	1	50	50	13.37	0.00	32.43	2.3	0.7	61.99
25FA	2	1	25	75	6.72	0.00	53.33	2.3	0.7	63.49
100RHA	2	1	0	100	0.00	0.00	74.23	2.3	0.7	64.98

2.3 Testing procedure

The direct compressive strength of hardened geopolymer paste specimens was determined at the age of 7 and 28 days in a 3000kN capacity Servo-Hydraulic Computer Controlled Compression Testing Machine. In each case, three identical specimens were tested in accordance to ASTM C-109-20a [30] and average values were reported. All the physical parameters studied (bulk density, apparent porosity water absorption and sorptivity) were performed on 28 days cured specimens. 24-hour oven dried specimen at a temperature of 80°C were utilised for determination of bulk density and apparent porosity. Apparent porosity was measured using Archimedes principle in compliance with ASTM C-20-00(2015) [32]. ASTM C-642-13 [33] procedure was followed for determination of bulk density, water absorption of geopolymer specimens. Sorptivity test determines the rate of absorption by the phenomenon of capillary rise. The specimens were initially painted with water proof enamel paint on all sides except the bottom and top surfaces, so as to allow capillary uptake of water only from bottom. The slope of the linear portion of the curve between cumulative mass gained per exposed surface area and square root of time taken was reported as the sorptivity of the geopolymer paste [34].

X-ray diffraction analysis was made using D8 Advance (Bruker) XRD machine with Cu-Kα radiation with the following conditions: 40 kV, 30 mA. Powdered specimens used for XRD were scanned in the scan angle (2θ) range of 10^o to 80^o. Scanning was performed in continuous mode with step size of (2θ) of 0.02 and scan step time of 1 sec. The reflection positions and d-spacing were analysed by DiffractEVA program and phase identified with Powder Diffraction Files (PDF). Rietveld refinement [35, 36] were done with Fullprof software (version 27th November 2019) with 10 % wt. of corundum as internal standard to enable the quantitative analysis. The percentage of amorphous phase were calculated as 100 minus the summation of weight percent of all the crystalline phase [36]. The average crystalline size of the specimens was calculated using Scherrer's equation [37]. Microstructures were studied through field emission scanning electron microscope (FESEM) by Sigma 300, Carl Zeiss. Quantification of the elements present in the geopolymer paste were performed by Energy dispersion X-Ray Analysis (EDX) at an accelerating voltage of 20 kV. FTIR were recorded on powdered samples with a Perkin Elmer, Simultaneous Thermal Analyser STA 8000 device. Spectra were recorded in the range 400-4000cm^{-1} with a resolution of 4 cm^{-1} and 16 scans per spectrum.

3. Results and discussion

3.1 X-ray Diffraction Analysis (XRD)

Figure 3 presents XRD patterns of blended and unblended geopolymer specimens for comparison. The main peaks of 100FA specimen comprises mainly of quartz (PDF 01-070-7344) and mullite (PDF 01-079-1456). Peaks mainly of quartz (PDF 01-070-7344), cristobalite (PDF 00-039-1425), and zeolite X (PDF 00-012-0246) were noticed in the XRD spectra of 100RHA specimens.75FA shows peaks of mullite at 2Θ angle of 17.05°, 24.83°, 31.47°, 41.39°, 43.16° and 68.76°. Characteristic high intensity peak of quartz was detected at 27.19° along with peaks of zeolite X at 40.02°, 50.76° and cristobalite peak at 33. 81°. These characteristic peaks were present in all the other blended geopolymer specimens with varying intensities. The formation of zeolite is a simultaneous reaction along with geopolymerisation and also depends on chemical composition of raw materials, activators used and curing parameters [38].

Presence of zeolite X were also reported in geopolymer precursor rich in silica and activated with sodium aluminate [28] and blended geopolymers (FA and RHA) [23]. Averaged

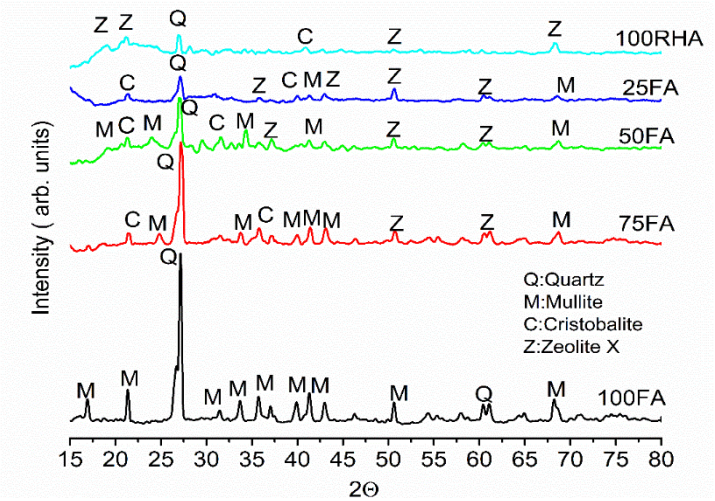

Figure 3 XRD of geopolymer specimen

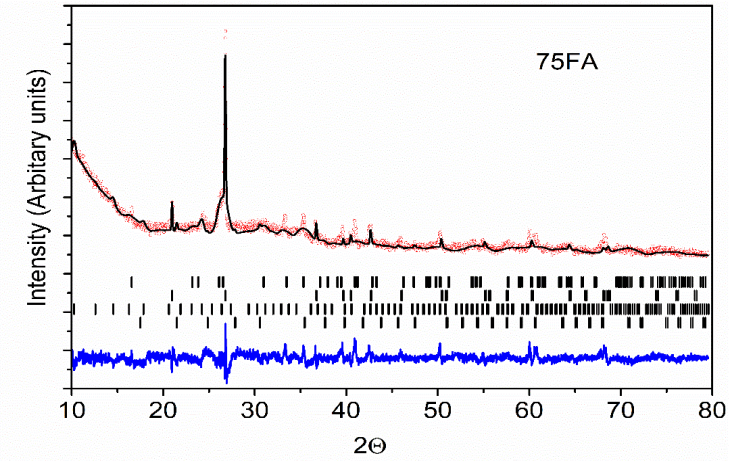

Figure 4 Rietveld plot for 75FA geopolymer

Table 3 Rietveld quantification of geopolymer specimens (%weight)

Specimen	Mullite	Quartz	Zeolite X	Cristobalite	Amorphous
100FA	12.40	19.86	-	-	67.74
75FA	9.95	15.67	0.85	0.92	72.60
50FA	8.52	9.85	1.86	1.95	77.82
25FA	3.13	7.71	4.92	5.07	79.17
100RHA	-	1.35	8.31	1.33	89.01

crystalline size of zeolite X calculated as per Scherrer's equation were 15.91, 18.66, 18.89 and 19.2 nm for 75FA, 50FA, 25FA and 100 RHA respectively. Decreasing trend in the intensity of quartz peak was detected for all the blended and RHA geopolymer specimens at approximately 2Θ angle of 27° in comparison to that of 100FA. It has been related to increase formation of amorphous geopolymer gel with increasing percentage RHA in the specimen [39]. The different crystalline phases and zeolite formation as well as the amorphous phase of the geopolymer specimens are tabulated in Table 3.

Unblended geopolymer specimen 100FA has amorphous content of about 67.74% with crystalline components of mullite (12.40%) and quartz (19.86%). As RHA is blended with FA, the crystalline percentage tend to decrease leading to the growth of amorphous content of the blended geopolymer specimen (67.74-89.01%). The amorphous content of 75FA shows an enhancement of about 7.17% over that of 100FA.Blended geopolymer also shows considerable growth in the formation of zeolite X from 0.85-8.31% with increasing RHA in the blending.

This may be due to the increased amorphous silica supplement from RHA blended as well as production of more amorphous geopolymer gel [25, 40, 41].Typical XRD Rietveld plot for 75FA geopolymer specimen is shown in Figure 4. The black and red spectra indicate measured and calculated patterns respectively while the blue spectra specify the residual between these two patterns. The positions of Bragg peaks for different phases are denoted by the marks shown in Figure 4. The quality of the fit is adjusted by the weighted profile factor (R_{wp}) [35] which are in the range of 10.78-11.45% for all the geopolymer specimens.

3.2 FESEM and EDX analysis

Figure 5(a)-(e) shows micrographs of geopolymer specimens. Occurrence of few voids with regular and smooth texture is noticed for 100FA specimen. Micrograph of 100RHA shows irregular and flaky nature similar to that of raw RHA in Figure 2 (a).

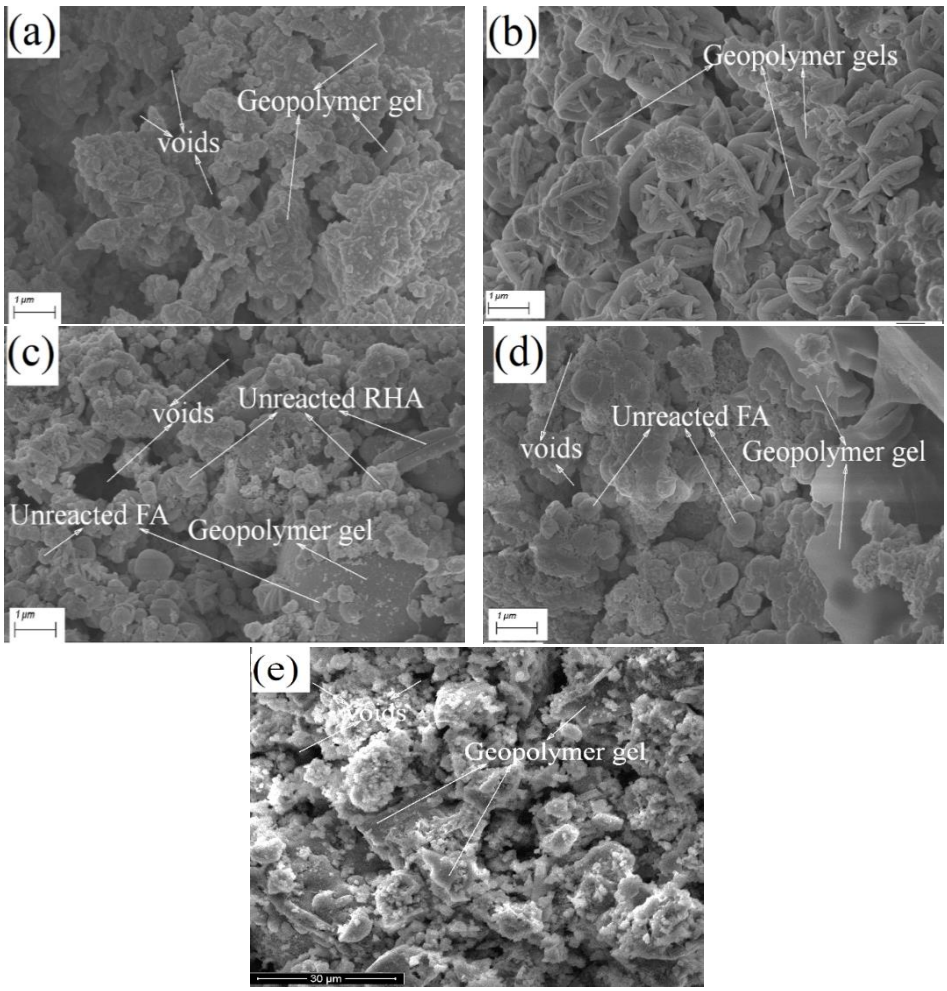

Figure 5 SEM micrographs (a) 100FA (b) 75FA (c) 50FA (d) 25FA (e) 100RHA

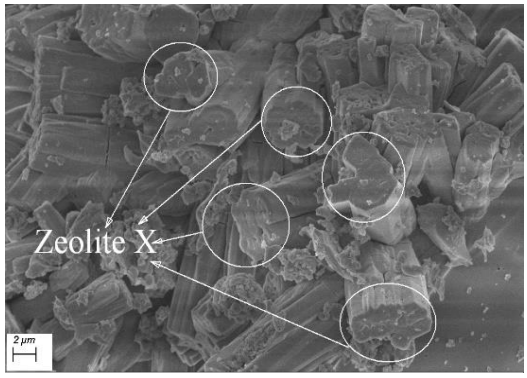

Figure 6 SEM micrograph of Zeolite X

It is observed that voids in the gel matrix of blended geopolymer were much lesser than those of unblended geopolymer. The microstructure of 75FA with 25% replacement by RHA present significant densification of geopolymer matrix. The comparatively smaller particle size of RHA (d_{50}=37.58µm and d_{90} =73.64µm) gets dissolved to form more gel phase while also filling up the voids in the geopolymer matrix. Previous researchers had stated the same phenomenon of filler effect of RHA in geopolymer matrix [25, 41]. It can be also be construed that blending of RHA plays a positive role in the improvement of pore structure of the geopolymer gel matrix [41]. The amount of unreacted FA and RHA particle were also observed to be higher for 50FA and 25FA as compared to 75FA specimen. Figure 5(c) for 50FA specimen shows spherically shaped unreacted /partially reacted fly ash which adhered on the surface of the geopolymer gel. Elongated and flaky shaped particle in the micrograph are attributed to unreacted RHA. The amount of unreacted RHA are relatively lower for 25FA specimen though spherical shaped unreacted FA were still apparent from Figure 5(d). The unreacted FA and RHA are assumed to have not participated in the geopolymerisation process. Silicate and aluminum geopolymer precursors from FA and RHA are transformed by optimal kinetic reaction into aluminosilicate gel and crystalline zeolite phase [42]. The formation of zeolite X were also confirmed by XRD as discussed in the previous section. SEM micrograph can detect occurrence of small crystals as shown in Figure 6 with magnification of 25000x and scale bar of 2µm.The microstructure shows moderately altered octahedral shaped individual crystals on the surface of the geopolymer gel. Previous literature also reported zeolite X to have octahedral morphological structure [43, 44].

The average results of five different points for EDX analysis of geopolymer specimens is presented in Table 4. The main contributing weight percentage are of elements: Silicon (Si), Aluminum (Al), Sodium (Na), Iron (Fe), Calcium (Ca), and Oxygen (O). The ratio of Si/Al and Na/Al were found to have slightly deviated from the initial ratio of 2 and 1 respectively taken during preparation.100FA specimens have Si/Al and Na/Al ratios of 1.97 and 0.75 respectively. The slight decrease in ratio is attributed to the swift dissolution of alumina from the raw fly ash [45]. Moreover, thermal curing at relatively high temperature for a long period results in higher dissolution and nucleation process of Al [42]. For unblended 100RHA, Si/Al ratio of 100RHA was found nearly equal to that of original batch composition. This validates that sodium aluminate can be utilized as the source of alumina in the geopolymer matrix.

Table 4 EDX weight Percentage analysis of geopolymer specimens.

Element	100FA	75FA	50FA	25FA	100RHA
O	40.61	43.46	43.52	43.94	41.82
Na	17.33	13.95	10.86	12.72	13.49
Al	12.96	12.49	12.87	12.54	12.34
Si	25.47	26.93	29.22	29.66	25.5
K	0.36	0.48	0.95	0.33	1.97
Ca	0.35	0.44	1.24	0.61	2.78
Ti	0.61	0.82	0.26	0.03	1.12
Fe	2.31	1.43	1.08	0.17	0.98
Si/Al	1.97	2.16	2.27	2.37	2.07
Na/Al	0.75	0.9	1.19	0.99	0.91

Table 5 Variation of characteristics FTIR bands

Specimen	Si-O-Si asymmetric vibration	Si-O-Si bending	D6R vibrational bands of Zeolite X	
100FA	977.39	-	-	-
75FA	988.64	555	670	743
50FA	1001.31	556	674	749
25FA	1008.75	558	677	752
100RHA	1012.21	560	678	756

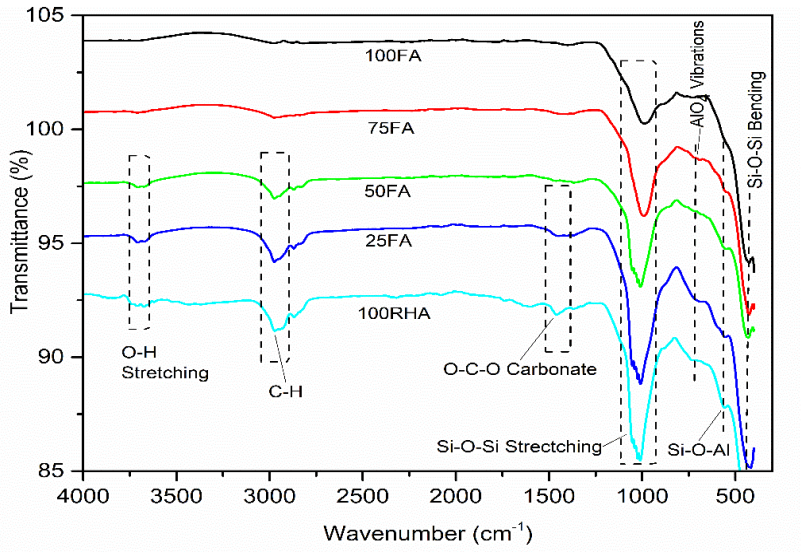

Figure 7 FTIR of geopolymer Specimens

For blended geopolymer, a growing trend of Si/Al ratio is observed as the percentage replacement of FA with RHA is increased. Si/Al ratios of 2.16, 2.27 and 2.37 corresponding to 75FA, 50FA and 25FA respectively were detected. The rate of release of alumina was reported to be faster for specimens containing sodium aluminate [26]. However, the released Al creates a siliceous layer on the surface of FA particle which hinders the dissolution of silica particles [26, 46]. This may be the reason for more unreacted FA and RHA particles observed in the SEM micrographs (Figure 5 b-d). It results in slightly higher value of Si/Al ratio as confirmed by the EDX analysis.

3.3 Fourier Transform Infrared Radiation (FTIR)

FTIR spectra of geopolymer specimens are presented in Figure 7. Geopolymer specimen of 100RHA exhibits strong peaks corresponding to Si-O-Si asymmetric vibration at approximately 1017 cm^{-1}.Peaks at 2970 $cm^{-1}$and 1470 cm^{-1} are credited to C-H [47] and O-C-O [29] respectively. The occurrence of O-C-O peak in the FTIR spectra suggested presence of sodium carbonate by reaction with atmospheric CO_2 [29]. Minor peaks were also observed at around 430 cm^{-1} and 560 cm^{-1} corresponding to Si-O-Si bending and Si-O-Al stretching and bending respectively [48]. The band near 730 cm^{-1} and 3690 cm^{-1} are allocated to AlO_4 vibration and O-H stretching bond.

For blended geopolymer, Si-O-Si asymmetric vibration were detected in the approximate range of 990-1013 cm^{-1} and approximately 980cm^{-1} for 100FA. The observed shift of Si-O-Si stretching to higher wavenumber as RHA is blended with FA indicate lengthening and reduction of bond angle signifying a chemical change in the geopolymer matrix [48]. The characteristic peaks of C-H (approx.2970 cm^{-1}) and O-H stretching (3690 cm^{-1}) were observed in 100RHA, 25FA and 50FA specimens. However, these peaks were absent in the case of 75FA and 100FA. This may be attributed to lesser extra water provided in these specimens as compared to the others. Si-O-Si bending varies from around 420-435 cm^{-1} for all the blended geopolymers. The bands at approximately 670 and 750 cm^{-1} are assigned to zeolite X [49, 50]. The band at approx. 570 cm^{-1} also corresponds to vibrations of double rings (D6R) [51]. The presence of these band in 100RHA, 25FA, 50FA and 75FA authenticate presence of zeolite X as observed in SEM micrograph and discussed in XRD. The variation of the main band Si-O-Si asymmetric vibration, Si-O-Si bending and D6R vibrational bands are tabulated in Table 5.

Increasing trend was observed in the main peak Si-O-Si asymmetric vibration band and Si—Si bending band as the

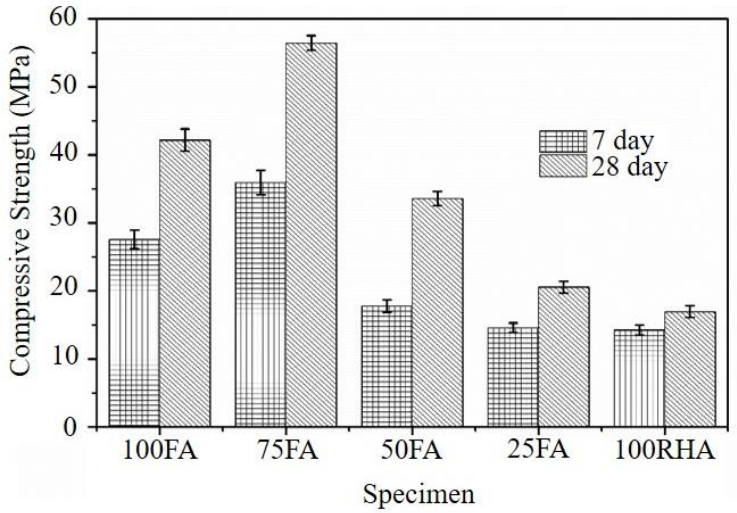

Figure 8 Compressive Strength of geopolymer specimens

blending percentage by RHA is increased. 100FA does not show the spectra corresponding to Si-O-Si bending. Increase in vibrational band is reported to be indirectly associated with more crystallization phase of zeolite [50] validating the percentage increase presented in Table 3.

3.4 Compressive strength

Compressive strength of geopolymer specimens after 7 and 28 days of curing are shown in Figure 8. Irrespective of the blending percentage, geopolymer specimens shows an increasing trend as the curing days were varied from 7 to 28 days. The initial first week strength were about 52-84 % of the strength observed after four weeks. This is due to faster dissolution rate of alumina from sodium aluminate during the initial week which significantly influences the mechanical strength. Aluminum contributes to the formation of cross linking of the gel- formation and provides mechanical integrity for initial strength development of the geopolymer specimens [26]. RHA particles release silica in a much slower rate as compared to the alumina. This affected the initial geopolymer reaction with inadequate silicate to react with aluminum and sodium [26]. The amount of soluble silica increases in the later weeks resulting in enhanced gel formation causing further development of mechanical strength.

The finer particles of RHA filled the voids present in the geopolymer matrix which densify the specimen and lead to higher mechanical strength [25]. The relatively denser matrix was also observed in the SEM micrographs of 75 FA in Figure 5(b). Blending of RHA with FA decreased the peaks of major crystalline phases in the geopolymer specimen. This is evident from the XRD pattern as well as the quantitative analysis of the XRD. The decrease in crystalline intensity indicates the formation of more amorphous geopolymer gel which have been reported to increase the compressive strength [36, 52]. An increase of 7.17 % is observed in the amorphous content of 75FA over 100FA geopolymer as indicated in Table 3. The strength development of geopolymer specimens studied show 75FA with highest value of 35.95 and 56.43MPa after 7 and 28 days respectively. This is about 30.39 and 33.81% enhancement over unblended fly ash based geopolymer specimen. However, a decreasing trend in compressive strength were observed in geopolymer specimens when percentage replacement by RHA is beyond 25%. Previous studies on FA and RHA blended geopolymer reported optimum replacement of RHA at 20% [24] and 35% [23]. Reduction of 20.41, 51.2 and 59.78% in 28 days compressive strength as compared to 100FA were noticed for 50FA, 25FA and 100RHA respectively. The decreasing trend in compressive strength may be related with other synthesis parameters which might have influenced the mechanical strength.

One of the factors influencing the compressive strength might be addition of extra water. Incorporation of RHA in the synthesis of blended geopolymer increases the water demand of the geopolymer paste to make it workable. This leads to lower alkalinity of the activator, slower rate of reaction and development of a more porous microstructure [28]. Moreover, the formation of zeolite X also effect the strength development of the geopolymer specimen. The presence of zeolite X in blended and 100RHA specimens has been confirmed by XRD, SEM and FTIR analysis. The transformation of amorphous gel into zeolites reorganized the geopolymer matrix and can influence the compressive strength of the specimens. Quantitative XRD phrase analysis indicates an increasing trend of formation of zeolite X as RHA is blended with FA. Optimal level of zeolite X enhances the compressive strength of the geopolymer matrix beyond which it has an impeding effect [53]. The difference in microstructure of zeolite and geopolymer hampers the development of compressive strength. Zeolite have microporous structure based on 3D cage system which is different from 3D tetrahedral network of aluminum and silicon of geopolymers [7]. The averaged crystalline size of zeolite X have been found to increase as calculated using Schneir equation with higher percentage blending by RHA in the geopolymer. The crystalline size of the zeolite X has a negative effect as it decrease the compressive strength of the blended geopolymer specimens. Similar correlation was also highlighted by Takeda et al [37].

3.5 Physical properties

Bulk density and apparent porosity for geopolymer paste specimens are presented in Figure 9. 75FA specimens with 25% blending by RHA results in highest bulk density of 1.81 g/c.c. when compared with those of other the geopolymer specimens. Bulk density decreases significantly as the percentage blending by RHA is increased. However, blended geopolymer exhibit a reverse trend in case of apparent porosity with 75FA specimen showing least value of 7.15%. This amounts to about 25% improvement over that of unblended FA geopolymer. Apparent porosity increases remarkably with RHA percentage in the specimen. On comparison with that of 100FA specimens, bulk density decreased at 5.67, 8.05 and 12% for 50FA, 25FA and 100RHA respectively.

Apparent porosity was found to increase exponentially for 25FA and 100RHA geopolymer respectively at 35.86 and 34.32 %.

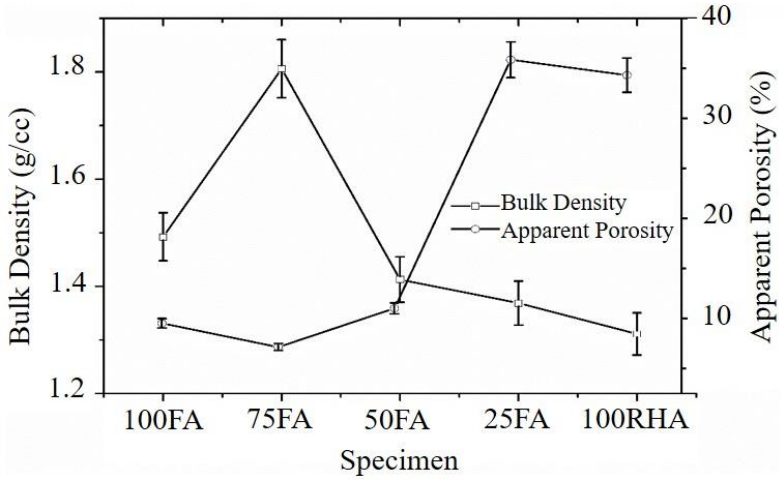

Figure 9 Bulk Density and Apparent Porosity of geopolymer

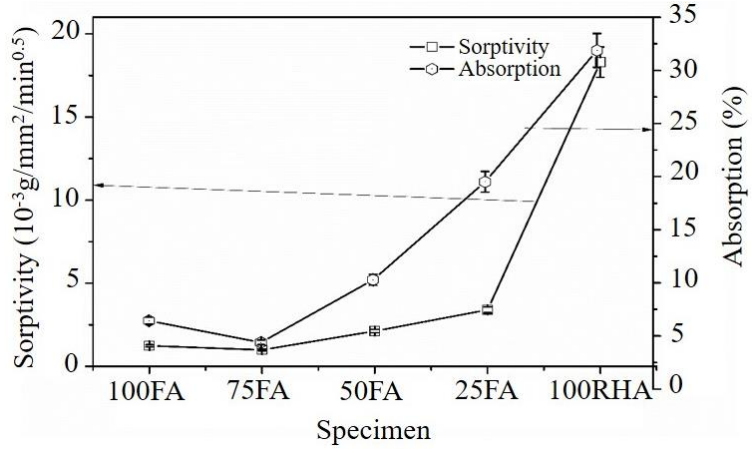

Figure 10 Water Sorptivity and Water absorption of geopolymer

Water absorption and sorptivity for geopolymer specimens are highlighted in Figure 10. Sorptivity and water absorption varies in a similar trend with a least value of 0.99 x 10^{-3} g/mm^2/min$^{0.5}$ and 4.39% respectively for 75FA geopolymer specimen.

75FA have around 32% and 20.16% improvement over unblended FA geopolymer for sorptivity and water absorption respectively. Beyond 25% RHA blending in geopolymer, both the parameters noticeably increased. The best physical properties of 75FA translate to its highest compressive strength among the geopolymer specimen. The effective combination of RHA with FA leads to formation of denser matrix of geopolymer matrix through filling effect and enrichment of the gel as validated by the SEM micrographs. Similar observations were also reported for RHA blended geopolymer [25, 54]. Further increase in blending percentage of RHA has a negative effect on all the physical parameters studied. This could be due to the porous microstructure of the RHA itself [54]. The poor dispersion and agglomeration phenomenon are attributed for the observed negative effect on these parameters [40, 55].

4. Conclusions

Based on the experimental results, the following were drawn

1. Sodium aluminate as aluminum (Al) additive for the geopolymer reaction of blended geopolymer based on fly ash and rice husk ash is established.
2. The optimal replacement percentage of FA with RHA was 25% as indicated by the highest compressive strength (56.43MPa) over all the geopolymer specimen studied. It was further supported by results of physical parameters such as bulk density, water absorption, sorptivity and apparent porosity.
3. SEM micrographs of 75FA (25% RHA) validates its observed best properties with denser matrix as compared to other specimens. Finer particles of RHA in the specimen sufficiently fills the voids in the geopolymer matrix leading to improved properties.
4. Quantitative XRD reveals the progressive growth of zeolite X along with the aluminosilicate gel as the percentage blending of RHA is increased. SEM micrographs and FTIR spectra also established the presence of zeolite X.
5. Optimal formation of zeolite X enhances the compressive strength beyond which it has a negative effect on blended geopolymer.
6. FA and RHA are found suitable for making blended geopolymer of desired properties by properly adjusting the quantity of water for achieving good workability.

5. Funding source

This research did not receive any specific grant from funding agencies in the public, commercial, or not-for-profit sectors.

6. References

[1] Davidovits J. Geopolymers: Inorganic polymeric new materials. J Therm Anal. 1991;37:1633-56.

[2] Davidovits J. Global warming impact on the cement and aggregates industries. World Resource Rev. 1994;6(2):263-78.
[3] Thokchom S, Ghosh P, Ghosh S. Durability of fly ash geopolymer mortars in nitric acid–effect of alkali (Na_2O) content. J Civ Eng Manag. 2011;17(3):393-9.
[4] Thokchom S, Ghosh P, Ghosh S. Effect of Na_2O content on durability of geopolymer pastes in magnesium sulfate solution. Can J Civ Eng. 2012;39(1):34-43.
[5] Kumar S, Kumar R. Mechanical activation of fly ash: effect on reaction, structure and properties of resulting geopolymer. Ceram Int. 2011;37(2):533-41.
[6] Luukkonen T, Abdollahnejad Z, Yliniemi J, Mastali M, Kinnunen P, Illikainen M. Alkali-activated soapstone waste - mechanical properties, durability, and economic prospects. Sustain Mater Tech. 2019;22:1-8.
[7] Istuque DB, Reig L, Moraes JCB, Akasaki JL, Borrachero MV, Soriano L, et al. Behaviour of metakaolin-based geopolymers incorporating sewage sludge ash (SSA). Mater Lett. 2016;180:192-5.
[8] Steinerova M. Mechanical properties of geopolymer Mortars in relation to their porous structure. Ceramics-Silikáty. 2011;55(4):362-72.
[9] Glid M, Sobrados I, Rhaiem HB, Sanz J, Amara ABH. Alkaline activation of metakaolinite-silica mixtures: Role of dissolved silica concentration on the formation of geopolymers. Ceram Int. 2017;43(15):12641-50.
[10] Jithendra C, Elavenil S. Effects of silica fume on workability and compressive strength properties of aluminosilicate based flowable geopolymer mortar under ambient curing. Silicon. 2020;12:1965-74.
[11] Rattanasak U, Chindaprasirt P, Suwanvitaya P. Development of high volume rice husk ash alumino silicate composites. Int J Miner Metall Mater. 2010;17(5):654-9.
[12] Goriparthi MR, Gunneswara Rao TD. Effect of fly ash and GGBS combination on mechanical and durability properties of GPC. Adv Concr Construct. 2017;5(4):313-30.
[13] Yazdi MA, Liebscher M, Hempel S, Yang J, Mechtcherine V. Correlation of microstructural and mechanical properties of geopolymers produced from fly ash and slag at room temperature. Construct Build Mater. 2018;191:330-41.
[14] El-Gamal SMA, Selim FA. Utilization of some industrial wastes for eco-friendly cement production. Sustain Mater Tech. 2017;12:9-17.
[15] Nimwinya E, Arjharn W, Horpibulsuk S, Phoo-ngernkham T, Poowancum A. A sustainable calcined water treatment sludge and rice husk ash geopolymer. J Clean Prod. 2016;119:128-34.
[16] Saxena SK, Kumar M, Singh NB. Influence of alkali solutions on properties of pond fly ash-based geopolymer mortar cured under different conditions. Adv Cement Res. 2018;30(1):1-7.
[17] Shaikh F, Haque S. Effect of nano silica and fine silica sand on compressive strength of sodium and potassium activators synthesised fly ash geopolymer at elevated temperatures. Fire Mater. 2018;42(3):324-35.
[18] Srinivasa Rao C, Subha Lakshmi C, Tripathi V, Dubey RK, Sudha Rani Y, Gangaiah B. Fly ash and its utilization in indian agriculture: constraints and opportunities. In: Ghosh SK, Kumar V, editors. Circular Economy and Fly Ash Management. Singapore: Springer; 2020. p. 27-46.
[19] Central Electricity Authority. CEA Annual report 2018-19. New Delhi: Central Electricity Authority; 2019.
[20] FAO. World Food and Agriculture – Statistical pocketbook 2019. Rome: Food and Agriculture Organization of the United Nations (FAO); 2019.
[21] Fletcher RA, MacKenzie KJD, Nicholson CL, Shimada S. The composition range of aluminosilicate geopolymers. J Eur Ceram Soc. 2005;25(9):1471-7.
[22] Shyamananda SN, Suresh T, Rama D. Characteristics of rice husk ash–sodium aluminate geopolymer at elevated temperature. Emerg Mater Res. 2020;9(1):1-8.
[23] Hwang CL, Huynh TP. Effect of alkali-activator and rice husk ash content on strength development of fly ash and residual rice husk ash-based geopolymers. Construct Build Mater. 2015;101:1-9.
[24] Detphan S, Chindaprasirt P. Preparation of fly ash and rice husk ash geopolymer. Int J Miner Metall Mater. 2009;16(6):720-6.
[25] Nazari A, Bagheri A, Riahi S. Properties of geopolymer with seeded fly ash and rice husk bark ash. Mater Sci Eng A. 2011;528(24):7395-401.
[26] Hajimohammadi A, Provis JL, van Deventer JSJ. Effect of alumina release rate on the mechanism of geopolymer gel formation. Chem Mater. 2010;22(18):5199-208.
[27] Phair JW, Deventer JSJv. Characterization of fly-ash-based geopolymeric binders activated with sodium aluminate. Ind Eng Chem Res. 2002; 41(17):4242-51.
[28] Hajimohammadi A, van Deventer JSJ. Solid reactant-based geopolymers from rice hull ash and sodium aluminate. Waste Biomass Valorization. 2016;8(6):2131-40.
[29] Sturm P, Gluth GJG, Brouwers HJH, Kühne HC. Synthesizing one-part geopolymers from rice husk ash. Construct Build Mater. 2016;124:961-6.
[30] ASTM. ASTMC109/C109M-20a. Standard test method for compressive strength of hydraulic cement mortars (using 2-in. or [50-mm] cube specimens). West Conshohocken: ASTM International; 2020.
[31] Thakur RN, Ghosh S. Effect of mix composition on compressive strength and microstructure of fly ash based geopolymer composites. ARPN J Eng Appl Sci. 2009;4(4):68-74.
[32] ASTM. ASTMC20-00. Standard test methods for apparent porosity, water absorption, apparent specific gravity, and bulk density of burned refractory brick and shapes by boiling water. West Conshohocken: ASTM International; 2015.
[33] ASTM. ASTMC642-13. Standard test method for density, absorption, and voids in hardened concrete. West Conshohocken: ASTM International; 2013.
[34] Sabir BB, Wild S, O'Farrell M. A water sorptivity test for mortar and concrete. Mater Struct. 1998;31:568-74.
[35] Fernández-Jiménez A, de la Torre AG, Palomo A, López-Olmo G, Alonso MM, Aranda MAG. Quantitative determination of phases in the alkaline activation of fly ash. Part II: Degree of reaction. Fuel. 2006;85(14-15):1960-9.
[36] Bhagath Singh GVP, Subramaniam KVL. Quantitative XRD study of amorphous phase in alkali activated low calcium siliceous fly ash. Construct Build Mater. 2016;124:139-47.
[37] Takeda H, Hashimoto S, Yokoyama H, Honda S, Iwamoto Y. Characterization of zeolite in zeolite-geopolymer hybrid bulk materials derived from kaolinitic clays. Materials (Basel). 2013;6(5):1767-78.
[38] Ng C, Alengaram UJ, Wong LS, Mo KH, Jumaat MZ, Ramesh S. A review on microstructural study and compressive strength of geopolymer mortar, paste and concrete. Construct Build Mater. 2018;186:550-76.
[39] Irfan Khan M, Azizli K, Sufian S, Man Z. Sodium silicate-free geopolymers as coating materials: effects of Na/Al and water/solid ratios on adhesion strength. Ceram Int. 2015;41(2):2794-805.
[40] Assaedi H, Shaikh FUA, Low IM. Influence of mixing methods of nano silica on the microstructural and mechanical properties of flax fabric reinforced geopolymer composites. Construct Build Mater. 2016;123:541-52.

[41] Liang G, Zhu H, Zhang Z, Wu Q. Effect of rice husk ash addition on the compressive strength and thermal stability of metakaolin based geopolymer. Construct Build Mater. 2019;222:872-81.
[42] Kusbiantoro A, Nuruddin MF, Shafiq N, Qazi SA. The effect of microwave incinerated rice husk ash on the compressive and bond strength of fly ash based geopolymer concrete. Construct Build Mater. 2012;36:695-703.
[43] Yao G, Lei J, Zhang X, Sun Z, Zheng S. One-Step hydrothermal synthesis of zeolite X powder from natural low-grade diatomite. Materials (Basel). 2018;11(6):1-14.
[44] Kurniawan RY, Romadiansyah TQ, Tsamarah AD, Widiastuti N. Synthesis of zeolite-X from bottom ash for H_2 adsorption. IOP Conf Ser Mater Sci Eng. 2018;299: 012083.
[45] Pietersen HS, Fraay ALA, Bijen JM. Reactivity of fly ash at high pH. MRS Proceedings. 1989;178:139.
[46] Rees CA, Provis JL, Lukey GC, van Deventer JSJ. The mechanism of geopolymer gel formation investigated through seeded nucleation. Colloid Surface Physicochem Eng Aspect. 2008;318(1-3):97-105.
[47] Huang Y, Gong L, Pan Y, Li C, Zhou T, Cheng X. Facile construction of the aerogel/geopolymer composite with ultra-low thermal conductivity and high mechanical performance. RSC Adv. 2018;8(5):2350-6.
[48] Chindaprasirt P, Jaturapitakkul C, Chalee W, Rattanasak U. Comparative study on the characteristics of fly ash and bottom ash geopolymers. Waste Manag. 2009;29(2):539-43.
[49] Rożek P, Król M, Mozgawa W. Geopolymer-zeolite composites: a review. J Clean Prod. 2019;230:557-79.
[50] Krol M, Minkiewicz J, Mozgawa W. IR spectroscopy studies of zeolites in geopolymeric materials derived from kaolinite. J Mol Struct. 2016;1126:200-6.
[51] Mozgawa W, Krol M, Barczyk K. FT-IR studies of zeolites from different structural groups. CHEMIK. 2011;65(7):667-74.
[52] Liew YM, Kamarudin H, Mustafa Al Bakri AM, Bnhussain M, Luqman M, Khairul Nizar I, et al. Optimization of solids-to-liquid and alkali activator ratios of calcined kaolin geopolymeric powder. Construct Build Mater. 2012;37:440-51.
[53] Alvarez-Ayuso E, Querol X, Plana F, Alastuey A, Moreno N, Izquierdo M, et al. Environmental, physical and structural characterisation of geopolymer matrixes synthesised from coal (co-)combustion fly ashes. J Hazard Mater. 2008;154(1-3):175-83.
[54] Liang G, Zhu H, Zhang Z, Wu Q, Du J. Investigation of the waterproof property of alkali-activated metakaolin geopolymer added with rice husk ash. J Clean Prod. 2019;230:603-12.
[55] Assaedi H, Shaikh FUA, Low IM. Effect of nano-clay on mechanical and thermal properties of geopolymer. J Asian Ceram Soc. 2018;4(1):19-28.